

# Spatial distribution of emission in Unidentified Infrared Bands from Midcourse Space Experiment Survey

S.K. Ghosh and D.K. Ojha

Tata Institute of Fundamental Research, Homi Bhabha Road, Mumbai (Bombay) 400 005, India

Accepted 12 March 2002

**Abstract.** Recently the Midcourse Space Experiment (MSX) has surveyed the Galactic plane in mainly four infrared bands between 6 and 25  $\mu\text{m}$ . Two of these bands cover several Unidentified Infrared emission Bands (UIBs). With the aim of extracting the spatial distribution of the UIB emission on a large scale, a scheme has been developed to model the MSX data with emission in the UIBs alongwith the underlying thermal continuum from the interstellar dust. In order to test this scheme, a sample of five Galactic compact H II regions (Sh-61, Sh-138, Sh-152, Sh-156, Sh-186; Zavagno & Ducci 2001) for which imaging study in some individual UIBs is available from ISOCAM measurements, has been studied. The results of this comparative study on small angular scale are as follows : (i) the morphological details extracted from our scheme agree very well with those from the superior ISOCAM measurements; (ii) the integrated strength of UIBs extracted from the MSX database correlates extremely well with the sum of the strengths of individual UIBs measured from ISOCAM. This tight correlation is very encouraging and promises the potential of MSX database for study of large scale spatial distribution of UIB emission (and the carriers of UIBs) in the entire Galactic plane.

**Key words.** Infrared : Interstellar medium : lines and bands – Infrared : Interstellar medium : H II regions

## 1. Introduction

The near to mid infrared spectrum originating from the interstellar medium of the Galactic star forming regions consists of various features in addition to a continuum. The continuum emission is attributed to the thermal emission from interstellar dust component and almost all narrow emission lines have been identified with atomic nebular, molecular, etc transitions originating from the interstellar gas component. In addition, several broader features have been detected which have been identified with features due to the solid state material of the dust (e.g. silicate absorption features at  $\sim 10$  and  $\sim 18 \mu\text{m}$  etc). There exists a class of broad emission features, sometimes called “Unidentified Infrared emission Bands” (UIBs; at 3.3, 6.2, 7.7, 8.6, 11.3, 12.7  $\mu\text{m}$ ), identity of whose carriers and the emission mechanisms are still a subject of active research. Some of these bands are widely believed to be characteristic of the bending and stretching modes of C=C and C-H bonds in aromatic molecules (e.g. fluorescent emission of Polycyclic Aromatic Hydrocarbons or PAHs; Leger & Puget 1984, Allamandola et al. 1985). However, other contenders also exist in literature (e.g. amorphous materials with aromatic hydrocarbon; Sakata et al. 1984, Borghesi et al. 1987). The study of large scale distribu-

tion of emission in the UIBs in the Galactic plane in general and selected star forming regions in particular would be important in understanding details of their emission mechanism.

The recent mission Infrared Space Observatory (ISO), in particular the imaging camera ISOCAM, has made it possible to study selected Galactic star forming regions in the UIBs. The ISOCAM instrument had several filters with the passbands selected to cover these UIBs (and also neighbouring continuum) so that emission in these individual features can be measured very precisely. However, it is unreasonable to expect Galactic plane surveys in UIB emission using the ISOCAM, since its primary objective was to achieve best possible (nearly diffraction limited) angular resolution in studies of individual astrophysical sources. As a result, largest single image from ISOCAM covers  $\sim 3' \times 3'$ .

With the advent of the Midcourse Space Experiment (MSX), new possibilities have emerged. The SPIRIT III instrument onboard MSX spacecraft, has surveyed the entire Galactic Plane ( $|b| < 5^\circ$ ) in four mid infrared bands centered around 8.3, 12.13, 14.65 and 21.34  $\mu\text{m}$  with an angular resolution  $\sim 18''$  (Price et al. 2001). These four bands are referred to as *A*, *C*, *D* and *E* spectral bands of MSX respectively (the SPIRIT III instrument also had two additional narrower bands at 4.29 and 4.35  $\mu\text{m}$ , called *B*<sub>1</sub> and *B*<sub>2</sub> bands). The usefulness of the MSX survey to

the study of diffuse interstellar medium and global characteristics has already been demonstrated (Cohen & Green 2001; Cohen 1999). The MSX band *A* includes the dominant UIB features at 6.2, 7.7 and 8.7  $\mu\text{m}$ . Similarly the MSX band *C* includes the UIB features at 11.3 and 12.7  $\mu\text{m}$ .

Whereas, the ISOCAM provides imaging capability in narrower spectral bands at higher angular resolution ( $3''$  or  $6''$ ) of selected regions, the MSX survey covers the entire Galactic plane in four broader bands (two of these covering several UIBs in addition to the continuum). Making use of this complementarity of ISOCAM vis a vis MSX, the following scheme has been explored to study large scale emission in the UIBs in the Galaxy :

- Model each picture element of MSX images with an integrated emission in UIB features superposed on a gray body continuum spectrum under some reasonable assumptions. The best fit solution (for each pixel) provides a measure of the UIB emission locally.
- Test the reliability of the above scheme by comparing the results of some selected Galactic star forming regions which have been studied using the ISOCAM and whose emission in individual UIBs have been quantified (e.g. Zavagno & Ducci 2001).
- The comparison should cover not only qualitative (e.g. structural details / morphology) aspects, but also quantitative correlation between the integrated estimate of UIB emission from our scheme and the ISOCAM results.

The section 2 describes the modelling scheme in detail, and the section 3 presents the results for the sample of six Galactic star forming regions using the MSX survey data. In section 4, a comparison between our results have been made with those from the ISOCAM by Zavagno and Ducci (2001). The conclusions are summarised in section 5.

## 2. The Scheme

The publicly available MSX Galactic plane survey radiance images (Infrared Processing and Analysis Center at <http://irsa.ipac.caltech.edu/applications/MSX>) in the four bands at 8.3 (*A*), 12.1 (*C*), 14.7 (*D*) and 21.3 (*E*)  $\mu\text{m}$  are gridded in  $6'' \times 6''$  pixel, though the true angular resolution is  $\sim 18.3''$  (Price et al. 2001), in the unit of  $Wm^{-2}sr^{-1}$ . The zodiacal background has already been subtracted out from these MSX survey maps. The spectrum emitted from each pixel is assumed to be a combination of a thermal continuum (modified Planck function or gray body) and the total radiance due to the relevant UIB features within the MSX band.

$$R_i = r_i^{UIBs} + \int (1 - e^{-\tau_\nu}) \times B_\nu(T) \times RSR_i(\nu) d\nu \quad (1)$$

$i = A, C, D, E$

where  $R_i$  are the measured radiances in the MSX bands.  $B_\nu(T)$  is the Planck function, and the term in parenthesis emulates the gray body spectrum emitted by the dust

grains.  $\tau_\nu$  is the optical depth due to the interstellar dust component at the frequency  $\nu$ . The functions  $RSR_i(\nu)$  represent the normalized relative spectral responses of the four MSX bands (Egan et al. 1999).

Since the range of frequencies covered by the MSX bands is limited, we assume a power law dependence of the dust emissivity on frequency, viz.,

$$\tau_\nu = \tau_{10} \times \left( \frac{\nu}{\nu_{10}} \right)^\beta. \quad (2)$$

here  $\tau_{10}$  is the optical depth at 10  $\mu\text{m}$  and  $\nu_{10}$  the frequency corresponding to wavelength 10  $\mu\text{m}$ . The value of  $\beta$  is a constant determined from the type of dust assumed. The effect of varying  $\beta$  is discussed later. The  $r_i^{UIBs}$  are the modelled total radiances in UIBs within the  $i$ -th MSX band. Since there are no known UIBs within the bands *D* and *E* of MSX,  $r_D^{UIBs} = 0$  and  $r_E^{UIBs} = 0$ . In addition, it has been assumed that the total radiance due to the UIBs in band *C* is proportional to that in band *A*, viz.,

$$r_C^{UIBs} = \alpha \times r_A^{UIBs}. \quad (3)$$

Here  $\alpha$  is held fixed to a reasonable value (based on available observational data and understanding) for all pixels of all star forming regions studied, though the effect of changing the value of  $\alpha$  has also been discussed later.

For each pixel on the sky with sufficient signal to noise ratio in each of the four MSX bands (implemented by map dynamic range cuts), we solve the set of four equations (eq. 1), for the three unknown variables viz.,  $T$ ,  $\tau_{10}$  and  $r_A^{UIBs}$ . A non-linear chi-square minimization scheme based on the finite difference Levenberg-Marquardt algorithm has been used for this purpose. The integrals in equation 1 are evaluated numerically using a cautious adaptive Romberg extrapolation method. In order to ensure that the best solution obtained indeed corresponds to a global minimum of chi-square, the computations are repeated for 125 different sets of initial guesses comprising of 5 values each of  $T$ ,  $\tau_{10}$  and  $r_A^{UIBs}$ . The grid of initial guess values for these three variables have been selected to cover a wide range of physical situations (e.g.  $T$  ranging between 50 and 800 K;  $\tau_{10}$  between  $10^{-6}$  and  $10^{-2}$ ;  $r_A^{UIBs}$  between  $10^{-7}$  and  $10^{-3} Wm^{-2}sr^{-1}$ ).

Invariably, the same solution is obtained starting from almost all different sets of initial guesses. The procedure is repeated for all pixels of the MSX map resulting in spatial distributions of these three physical variables. Here we extensively use the map of  $r_A^{UIBs}$ , which can be compared with the measurements from ISOCAM.

## 3. Results

### 3.1. Results from ISOCAM

#### 3.1.1. Available results from the literature & sample selection

From the literature we have selected the work of Zavagno and Ducci (2001; hereafter ZD) which is based on

ISOCAM measurements, for detailed comparison with results from our scheme of extracting emission in UIBs from the MSX data. The reason for selecting ZD is that they very uniformly studied (using same set of filters) a reasonable sample size comprising of five Galactic compact H II regions, viz., Sharpless(Sh)-61, Sh-138, Sh-152, Sh-156 and Sh-186. They studied the entire 3–12  $\mu\text{m}$  wavelength range accessible through ISOCAM. The ZD sample of compact H II regions are bright in IRAS 12  $\mu\text{m}$  band and are known to be strong emitters of UIBs at 7.7, 8.6 and 11.3  $\mu\text{m}$  but show no silicate absorption feature at 10 or 18  $\mu\text{m}$ . In addition, they represent a sequence in equivalent stellar type of the main exciting star.

Results of ZD are based on imaging with  $3'' \times 3''$  pixel mode of ISOCAM covering  $87'' \times 87''$  regions around Sh-61, Sh-152 & Sh-186 and  $174'' \times 87''$  around Sh-138 & Sh-156. Based on images in SW1 (centre  $\lambda$  : 3.57  $\mu\text{m}$ ;  $\lambda$  range : 3.05–4.10  $\mu\text{m}$ ; Césarsky et al. 1996), SW2 (3.30; 3.20–3.40), LW4 (6.00; 5.50–6.50), LW6 (7.75; 7.00–8.50), LW8 (11.4; 10.7–12.0) filters and five selected wavelengths using the CVF, they have quantified the UIB fluxes (actually radiances) in the 3.3, 6.2, 7.7 and 11.2  $\mu\text{m}$  features integrated over the mapped regions.

### 3.1.2. Our estimation of 7.7 $\mu\text{m}$ UIB feature emission

Using the publicly available ISOCAM data of the ZD sample sources (ISO Postcards from ISO Data Archive for General Users; <http://www.iso.vilspa.esa.es>), we have extracted the spatial distribution of emission in the 7.7  $\mu\text{m}$  UIB feature, using a method similar (but not identical) to ZD. First of all the underlying continuum at 7.7  $\mu\text{m}$  has been estimated from power law interpolation using the CVF images at 6.91 and 8.22  $\mu\text{m}$ . Next, this continuum has been subtracted from the LW6 image and the resulting emission has been attributed to the 7.7  $\mu\text{m}$  UIB (hereafter *UIB<sub>7.7</sub>* map). The resulting maps are presented and discussed in the next section.

## 3.2. Results obtained from the MSX survey

The MSX images of the five sources from ZD sample were processed following the scheme described above. The dust emissivity power law index  $\beta$  has been taken to be 1.0, which is commonly used in literature for general interstellar grains in the mid infrared wavelength region relevant to MSX bands (Scoville and Kwan 1976, Savage and Mathis 1979; Mathis 1990). However, other values of  $\beta$  have also been explored to ensure that the results obtained here are not sensitive to the choice of  $\beta$ , as discussed later.

### 3.2.1. Choice of $\alpha$

The value of  $\alpha$  represents the ratio of radiances in the UIBs within the passbands of MSX bands *C* and *A* (see eq. 3). These correspond to the features at 11.2 and 12.7  $\mu\text{m}$  (in band *C*) and at 6.2, 7.7 and 8.6  $\mu\text{m}$  (in band *A*). The value

of  $\alpha$  used here is based on the recent work by Verstraete et al. (2001) using the ISO-SWS. They have studied the 2.4 – 25  $\mu\text{m}$  spectra of three selected bright Galactic interstellar regions where dense molecular gas is illuminated by stellar radiation. Their wavelength range covers all the four MSX bands adequately. In addition, their choice of the three regions, viz., NGC 2023, Orion bar and M17-SW spans a wide range of excitation parameter (flux as well as hardness of the radiation field). The spectral resolution of the ISO-SWS measurements used by them was either 200 or 500, significantly large to resolve individual UIBs. The average value of  $\alpha$  for the above three regions representing different physical conditions, has been estimated by us from Fig.1 of Verstraete et al. (2001) to be 0.32 (with a very small dispersion). The effect of choosing different values of  $\alpha$  have been studied by us, which is discussed later.

From the study of Verstraete et al. (2001) it is clear that the contribution of forbidden ionic lines and molecular rotational lines, to the radiance within the MSX bands is negligible compared to the UIBs and the underlying continuum. Hence presence of these narrow lines should not affect our scheme of extracting the radiance due to the UIBs from the MSX data.

### 3.2.2. Maps of extracted UIB radiance

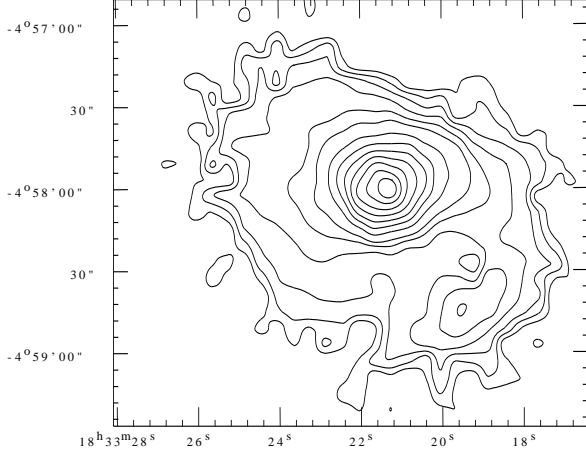
The extent of the angular region considered around each target was determined by the available dynamic ranges in the four MSX bands (i.e. only pixels satisfying the dynamic range condition in each band, were modelled). The usable dynamic range, *UDR*, for each band was defined from the frequency distribution of the radiance values,  $f(R)$ , in the corresponding map in the following manner :  $UDR = R_{max} / (R_{median} + R_{1/2}^-)$ , where  $R_{max}$  is the brightest pixel value,  $R_{median}$  is the median value of  $R$  as determined from  $f(R)$ , and  $R_{1/2}^-$  represents the brightness value satisfying  $f(R_{1/2}^-) = f(R_{median})/2$  and  $R_{1/2}^- < R_{median}$ . For a purely Gaussian distribution, the above translates to using the brightest  $\sim 15\%$  pixels of the full sample. It may be noted here that any particular choice of dynamic range only changes the outer boundary of the region where our scheme is applied by either including or excluding these pixels, without affecting any numerical results for other pixels. The details of the dynamic range used for the five regions are presented in Table 1.

The resulting integrated UIB radiance maps extracted by us from the MSX data for Sh-61, Sh-138, Sh-152, Sh-156 and Sh-186 are displayed in Figures 1 to 5 respectively as isophot contour plots. The sizes of these maps are selected based on the regions covered by the study by ZD. The peak UIB radiance values are also listed in Table 1.

Morphologically the extracted UIB radiance maps are very similar to the corresponding maps of thermal continuum emission from the dust grains, in general (at the scale of MSX resolution). However, there are differences between the spatial distribution of UIB emission and the

**Table 1.** Dynamic ranges of MSX maps and extracted peak  $UIB_A$  radiance

Source name	MSX Master Plate Number	Usable Dynamic Range				Peak( $UIB_A$ ) $W.m^{-2}.Sr^{-1}$
		Band A	Band C	Band D	Band E	
Sh-61	GP027.0+1.5	41	20	25	40	$7.74 \times 10^{-5}$
Sh-138	GP105.0+0.0	30	17	19	80	$8.35 \times 10^{-5}$
Sh-152	GP109.5-1.5	52	26	27	39	$5.82 \times 10^{-5}$
Sh-156	GP109.5+0.0	71	41	51	109	$9.93 \times 10^{-5}$
Sh-186	GP124.5+0.0	15	7.7	5.7	8.5	$1.70 \times 10^{-5}$

**Fig. 1.** The spatial distribution of total radiance in Unidentified Infrared emission Bands for the region around Sharpless 61, as extracted from the MSX maps. The contour levels are at 99, 90, 80, 70, 60, 50, 40, 30, 25, 20, 15, 10 & 5 % of the peak value of  $7.74 \times 10^{-5} W.m^{-2}.Sr^{-1}$ . The abscissa and the ordinate are R.A.(J2000.0) and Dec.(J2000.0) respectively.

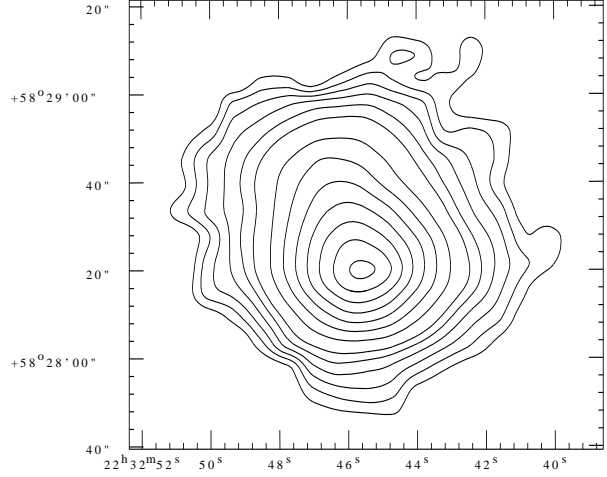
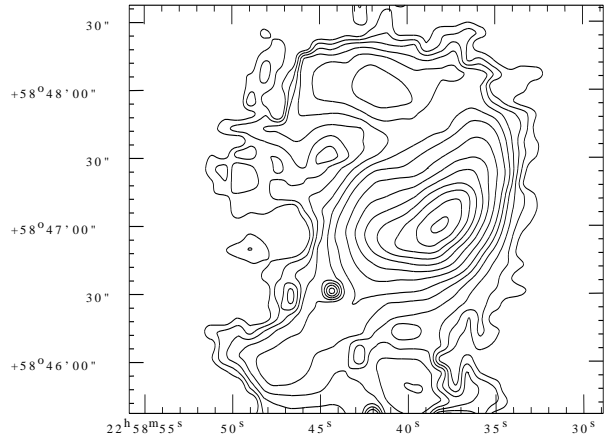
other modelled parameters, viz., the dust temperature and the optical depth corresponding to the thermal continuum emission. As one example, the map of dust optical depth ( $\tau_{10}$ , at  $10 \mu m$ ) for the Sharpless 152 region is presented in Figure 6, which can be compared with Figure 3.

#### 4. Comparison between MSX and ISOCAM results

##### 4.1. Morphological similarities

It is instructive to compare our maps from modelling of MSX data with those based on the ISOCAM data. Most relevant ISOCAM filters for this comparison are LW4, LW6 and LW8 covering the 6.2, 7.7 and  $11.2 \mu m$  UIBs. The former two features contribute to the UIB radiance in MSX band A and the last one in MSX band C.

The ISOCAM based  $UIB_{7.7}$  maps have been superposed (grey scale) on our integrated UIB map extracted from MSX maps, viz.  $r_A^{UIBs}$ , (hereafter  $UIB_A$ ), in Figures 7 to 11 corresponding to Sh-61, Sh-138, Sh-152, Sh-156

**Fig. 2.** Same as Fig. 1 but for Sharpless 138 region. The contour levels represent the same fractions of the peak as in Fig. 1. The peak here is  $8.35 \times 10^{-5} W.m^{-2}.Sr^{-1}$ .**Fig. 3.** Same as Fig. 1 but for Sharpless 152 region. The peak here is  $5.82 \times 10^{-5} W.m^{-2}.Sr^{-1}$ .

and Sh-186 respectively. For a more general comparison involving other UIBs, we refer to Figure 2 of ZD. In principle, our  $UIB_{7.7}$  map for each source must resemble LW6 map of ZD, which indeed is the case.

A marked morphological similarity between the contour plots corresponding to all these three ISOCAM filters

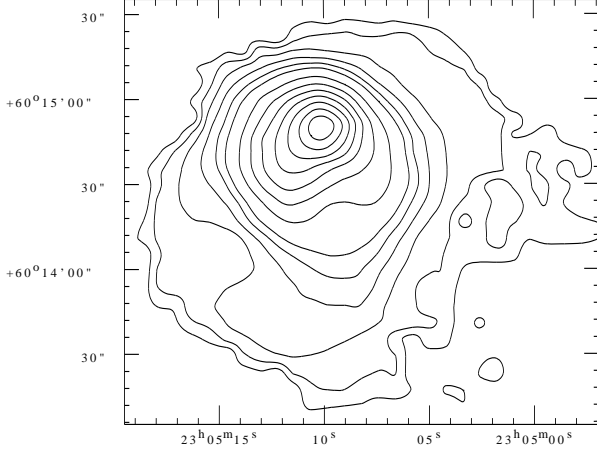


**Fig. 4.** Same as Fig. 1 but for Sharpless 156 region. The peak here is  $9.93 \times 10^{-5} W.m^{-2}.Sr^{-1}$ .

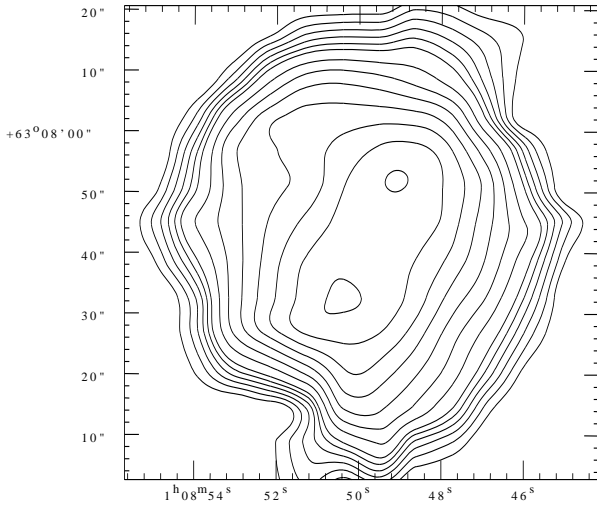


**Fig. 5.** Same as Fig. 1 but for Sharpless 186 region. The peak here is  $1.70 \times 10^{-5} W.m^{-2}.Sr^{-1}$ .

(LW4, LW6 & LW8) for all the five sources, support our assumption that  $r_C^{UIBs}$  and  $r_A^{UIBs}$  are correlated (equation 3). Next, we comment qualitatively about structural similarities between the spatial distribution of emission in individual UIBs as obtained from ISOCAM (our  $UIB_{7.7}$ ; LW4, LW6 & LW8 maps of ZD), vis a vis the total emission due to all UIBs within the MSX band A ( $UIB_A$ ). It may be noted that whereas ZD's maps represent intensity while ours are radiance. For qualitative comparison of structural details, it may be acceptable, however quantitative comparison is made in identical units later in this subsection.

#### 4.1.1. Sharpless 61

The peak position for Sh-61 in  $UIB_A$  map matches exactly with that of  $UIB_{7.7}$  (Fig. 7 here) / LW6 and LW4 (Fig.

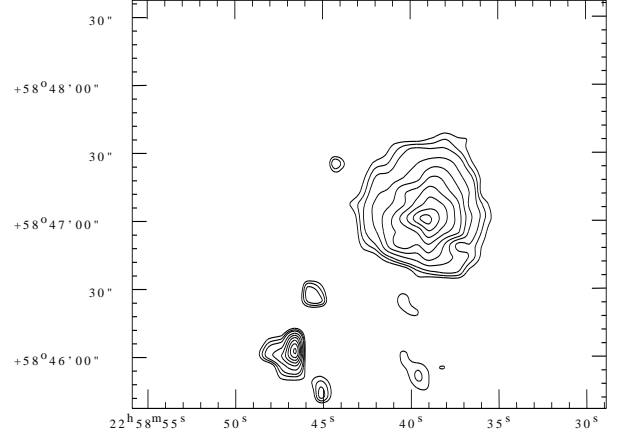


**Fig. 6.** The spatial distribution of dust optical depth ( $\tau_{10}$  at  $10 \mu m$ ) for the Sharpless 152 region. The contour levels are at 99, 90, 80, 70, 60, 50, 40, 30 & 20 % of the peak value of  $3.49 \times 10^{-4}$ . The structure of these contours differ from those of UIB radiance for the same region shown in Figure 3.

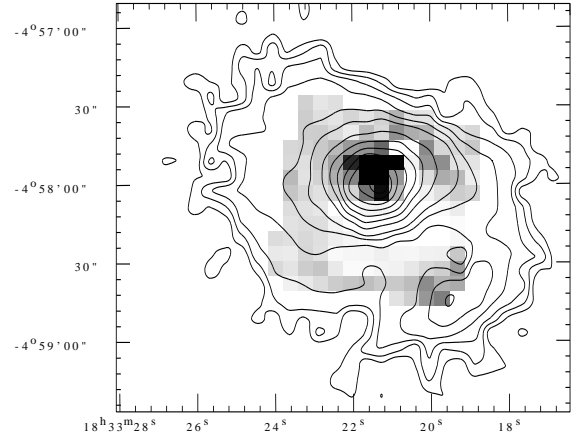


**Fig. 7.** Comparison of the total radiance in Unidentified Infrared emission Bands ( $UIB_A$ ; contours, same as in Fig. 1) as extracted from the MSX maps, with the emission in the  $7.7 \mu m$  UIB feature obtained from ISOCAM ( $UIB_{7.7}$  in grey scale; the grey scaled region also represents the area imaged by ISOCAM), for the region around Sharpless 61. The abscissa and the ordinate are R.A.(J2000.0) and Dec.(J2000.0) respectively.

2 of ZD). General structure of the  $UIB_A$  contours is also very similar to the maps LW4, LW6 as well as LW8 of ZD, with extension along E-W. We have detected an additional emission region due S-W from the main peak in the  $UIB_A$  map, which is perhaps barely below the lowest contour displayed in LW4 or LW6. However, our  $UIB_{7.7}$  map gives some hint of the same despite being near the edge of the ISOCAM field.

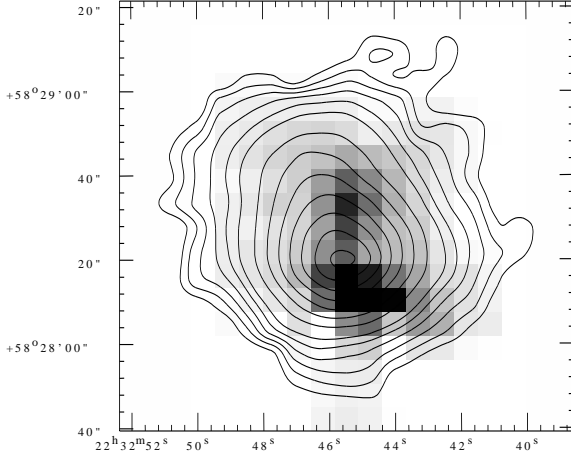


**Fig. 8.** Same as Figure 7, but for the Sharpless 138 region.

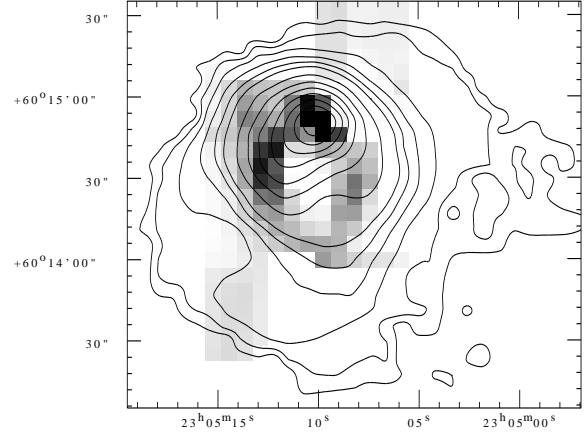


**Fig. 10.** Same as Figure 7, but for the Sharpless 156 region.

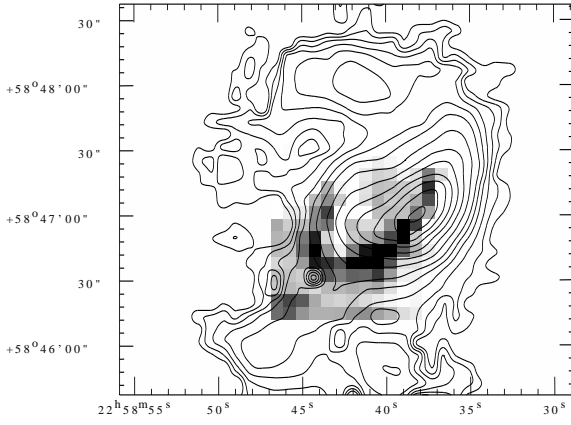


**Fig. 9.** Same as Figure 7, but for the Sharpless 152 region.

#### 4.1.2. Sharpless 138

For Sh-138 (Fig. 8), the  $UIB_{7.7}$  map has been able to resolve two components along N-S, and the  $UIB_A$  map shows the peak position as well as the contour shape consistent with that (note that the former has an angular resolution is  $\sim 18''$  while ISOCAM's is  $3''$ ). The contours in LW4, LW6 and LW8 maps are remarkably similar with a main peak and extension due north.

#### 4.1.3. Sharpless 152

Our  $UIB_{7.7}$  (Fig. 9) as well as the LW4, LW6 and LW8 maps for Sh-152 show very rich (but again similar between these filters) structure at an angular scale beyond the scope of MSX's resolution. Still, our  $UIB_A$  map for Sh-152 reproduces the major structures consistent with the above, viz., the curved shape extending approximately along S-E to N-W direction. The entire  $UIB_A$  map seems to be shifted by  $\sim 10''$  with respect to  $UIB_{7.7}$  map. Additional interesting structures are detected in our map (see Fig. 3;

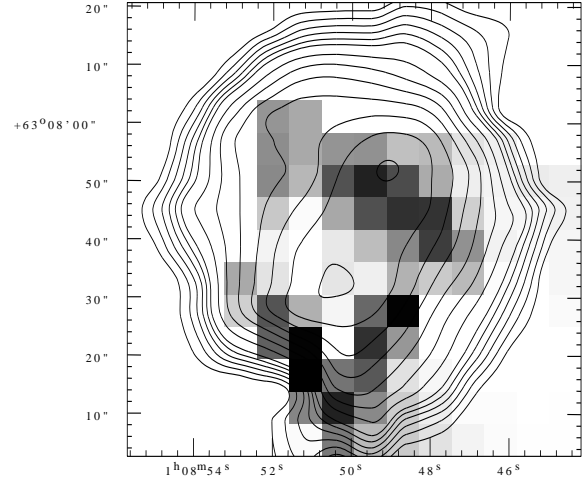


**Fig. 11.** Same as Figure 7, but for the Sharpless 186 region.

due north and due south with respect to the main peak) which lie outside the region mapped by ISOCAM.

#### 4.1.4. Sharpless 156

In the case of Sh-156 also the  $UIB_{7.7}$ , LW4, LW6 and LW8 maps show structural details at smaller angular scale which are unresolved in our  $UIB_A$  map (Fig. 10). But the curvature and density of contours in the latter indicate a morphology consistent with the above ISOCAM maps. The positions of respective peaks match very well in all these maps. UIB Emission is detected from a larger extended region all around the region mapped by ISOCAM, with one isolated secondary peak due west of the main peak (Fig. 4).

#### 4.1.5. Sharpless 186

The  $UIB_{7.7}$  as well as the  $UIB_A$  maps have resolved the Sh-186 region into two major peaks separated mainly along S-E to N-W line (Fig. 11). The stronger component being the S-E one in all maps. Similar structure is seen in the LW4, LW6 and LW8 maps too. The position of the peaks and other structural features also match very well (within  $< 10''$ ) between the  $UIB_A$  and all ISOCAM maps. The  $UIB_A$  map shows much more extended emission well outside the region mapped by ZD (Fig. 5).

#### 4.2. Quantitative correlation

In order to make quantitative comparison, the  $UIB_A$  radiance maps of the five regions have been integrated over the same corresponding regions as imaged by ZD, to get  $I(UIB_A^{MSX})$ . ZD have tabulated the solid angle integrated UIB fluxes  $F(3.3\mu m)$ ,  $F(6.2\mu m)$ ,  $F(7.7\mu m)$  and  $F(11.2\mu m)$  in their Table 4. We have compared their  $[F(6.2\mu m) + F(7.7\mu m)] = I(ISOCAM_{4+6})$  for each region with our integrated  $UIB_A$  radiances (see Table 2). Surprisingly, an extremely tight linear correlation has been found between  $I(ISOCAM_{4+6})$  and  $I(UIB_A^{MSX})$ ! It has been found that the ratio,  $\mathcal{R}_A = I(UIB_A^{MSX}) / I(ISOCAM_{4+6}) = 2.29 \pm 0.07$  (mean value and the error on the mean). This is despite several simplifying assumptions made in our analysis of the MSX data. This is indeed a remarkable finding, considering the very complex microscopic as well as macroscopic details that must go into deciding the amount of emission in the UIBs. Whereas the UIBs at 3.3, 8.6, 11.3 and 12.7  $\mu m$  originate from vibrational modes of the aromatic C–H bond, the bands at 6.2 and 7.7  $\mu m$  arise from the aromatic C–C bonds. There is strong evidence from the laboratory work on PAHs (carriers of UIBs), that the relative strengths of these features are very sensitive to the ionization state of the PAHs (Allamandola, Hudgins & Sandford 1999). Several observational studies of the spatial distribution of UIBs in well resolved H II regions support the same. Joblin et al. (1996) found that the ratio of 8.6  $\mu m$  to 11.3  $\mu m$  emission increases with the local far-UV (FUV) flux, which can ionize the PAH molecules. In a more recent study, Cr  t   et al. (1999) found similar variations in the ratio of UIB features for the M 17 complex. One possible explanation for the above correlation is as follows : (i) the angular sizes of the sample of sources considered here are such that the intrinsic resolution of MSX ( $\sim 18''$ ) spatially averages out various excitation effects expected close to the source of FUV radiation field; and (ii) the sample spans a somewhat limited range of FUV luminosity ( $\sim 2$ ). It may be interesting to extend the present work to nearby star forming regions for which the MSX resolution is adequate to probe the UIB emitting regions close to the exciting FUV source, and also covering a larger range of  $L_{FUV}$ .

In any case, our strong empirical correlation has many important and useful implications. For example, spatial distribution of emission in the UIBs for the entire Galactic

plane can be studied following our method and the MSX survey with an angular resolution  $\sim 20''$ . Of course the ISOCAM data provides the higher angular resolution information of selected regions and also the very important calibration factor above.

Since the band  $A$  of MSX includes the UIB at 8.6  $\mu m$  in addition to the ones at 6.2 and 7.7  $\mu m$ , it is natural to obtain a value for  $\mathcal{R}_A$  greater than unity. The mean value of  $\mathcal{R}_A$  so obtained can be interpreted in terms of the relative strength of 8.6  $\mu m$  feature vis a vis 6.2  $\mu m$  + 7.7  $\mu m$  features.

A similar correlation between  $UIB_C$  (which is just a scaled down value of  $UIB_A$ ) and the 11.2  $\mu m$  feature emission measured using ISOCAM (LW8) by ZD has been explored for our sample of five sources. The ratio,  $\mathcal{R}_C = I(UIB_C^{MSX}) / I(ISOCAM_8)$ , turns out to be  $2.98 \pm 0.28$ , which shows a much larger dispersion. In view of the fact that band  $C$  of MSX includes the UIB feature at 12.7  $\mu m$  also, the above is not surprising. The average value of  $\mathcal{R}_C$  should provide information regarding relative strengths of the features at 11.2 and 12.7  $\mu m$ . The larger dispersion in the values of  $\mathcal{R}_C$  among the five regions considered here, is perhaps indicative of the observed variability of the strength of 12.7  $\mu m$  feature vis-a-vis other UIBs at shorter wavelengths (e.g. among the sources whose ISO-SWS spectra have been presented by Verstraete et al. 2001).

Next, we discuss, how sensitive is the value of  $\mathcal{R}_A$  to the various assumptions made in analysing / modelling the MSX data. One of the parameters while modelling out the continuum from the MSX radiance in band  $A$ , is  $\beta$ , the dust emissivity index. Let us consider a few most popular types of dust grains, viz., Draine and Lee type (DL; Draine & Lee 1984), and Mathis, Mezger and Panagia (MMP; Mathis et al. 1983). One of the most popular dust size distribution is due to Mathis, Rumble and Nordsieck (MRN; Mathis et al. 1977). The MRN size distribution averaged values of absorption cross sections for DL and MMP type dust, for silicate and graphite grains have been computed earlier (Mookerjee & Ghosh 1999; Mookerjee et al. 1999). Using these for the MSX bands  $A$  to  $E$ , we find the effective value of  $\beta$  to be in the range 0.56 to 0.89. In any case, all calculations were repeated for the values of  $\beta = 0$  and 0.5 (in addition to 1.0). This had insignificant effect on the value of  $\mathcal{R}_A$ , and also the tightness of correlation between  $I(ISOCAM_{4+6})$  and  $I(UIB_A^{MSX})$ . It may be noted here that in case strong silicate absorption feature at  $\sim 9.8 \mu m$  was important, the above correlation could have been lost. The sample of ZD had been selected such that silicate feature is not visible in the IRAS LRS spectrum.

Another very important parameter in our scheme is  $\alpha$  (see equation 3), which has been held at a value of 0.32 on the basis of result of Verstraete et al. (2001). In order to study the sensitivity of our results on the numerical value of  $\alpha$ , we have repeated the calculations for a range of its values between 0 and 0.7. We find the following, for the value of  $\alpha$  between 0.15 and 0.35, the corre-

**Table 2.** Comparison of integrated radiances in UIBs obtained from ISOCAM measurements and those extracted by our scheme from MSX survey<sup>a</sup>

Source name	$I(\text{ISOCAM}_{4+6})^b$ $W.m^{-2}$	$I(\text{UIB}_A^{MSX})^c$ $W.m^{-2}$	$\mathcal{R}_A$
Sh-61	$1.64 \times 10^{-12}$	$4.00 \times 10^{-12}$	2.44
Sh-138	$1.50 \times 10^{-12}$	$3.12 \times 10^{-12}$	2.08
Sh-152	$1.74 \times 10^{-12}$	$3.88 \times 10^{-12}$	2.23
Sh-156	$2.20 \times 10^{-12}$	$5.56 \times 10^{-12}$	2.53
Sh-186	$3.83 \times 10^{-13}$	$8.38 \times 10^{-13}$	2.19

<sup>a</sup> Solid angle integration has been carried out over an identical region in both cases (ISOCAM & MSX).

<sup>b</sup> From Zavagno & Ducci (2001).

<sup>c</sup> Extracted from the MSX Galactic Plane Survey data using the scheme presented here.

lation between  $I(\text{ISOCAM}_{4+6})$  and  $I(\text{UIB}_A^{MSX})$  remains very tight, though the numerical value of  $\mathcal{R}_A$  changes slightly between 2.0 and 2.3. For values of  $\alpha$  outside this range (0.15–0.35), the correlation becomes much poorer and also the value of  $\mathcal{R}_A$  decreases on *either* side of this range! All of the above can be understood, if the total UIB feature strength in MSX bands *A* and *C* are really proportional. Hence we conclude that value of  $\mathcal{R}_A$  determined here is physically meaningful and should help quantifying the UIB emission in the Galactic plane in general.

## 5. Summary

A scheme has been developed to extract the contribution of Unidentified Infrared emission Bands (UIBs) from the mid infrared Galactic plane survey carried out by the SPIRIT III instrument onboard Midcourse Space Experiment (MSX) satellite in four bands. The scheme models the observations with a combination of thermal emission (gray body) from interstellar dust and the UIB emission from the gas component, under reasonable assumptions. Thus the spatial distribution of emission in the UIBs with an angular resolution  $\sim 20''$  (intrinsic to MSX survey) has been extracted.

In order to verify the reliability of this scheme, a detailed comparison has been made with the results obtained by Zavagno & Ducci (2001) using the ISOCAM instrument onboard Infrared Space Observatory (ISO), which has superior spectral and spatial resolutions than that of the MSX survey. Five Galactic star forming regions, viz., Sharpless 61 (Sh-61), Sh-138, Sh-152, Sh-156 and Sh-186, studied by Zavagno & Ducci (2001) have been used in this comparison.

The following results have been found :

- the UIB emission extracted from the MSX data is able to reproduce all major structural / morphological details detected by ISOCAM, consistent with its angular resolution;
- a very tight linear correlation has been found between the integrated UIB emission extracted from MSX data

and that obtained from ISOCAM data (hence MSX based UIB radiance estimates can be calibrated well); The above validates our assumption regarding emissivity law for interstellar dust grains and is self consistent with the assumed proportionality of UIB emission between the bands *A* and *C* of MSX. The correlation may be a result of spatial averaging over regions with different excitation details.

- the numerical value of the ratio of UIB radiances obtained from MSX and ISOCAM is an important information for understanding relative strengths of UIBs.

Hence, we conclude that our empirical scheme along with the MSX Galactic plane survey can be a powerful tool to study large scale spatial distribution of UIB carriers.

*Acknowledgements.* It is a pleasure to thank the referee Dr. M. P. Egan whose suggestions have improved the scientific content of this paper. This research made use of data products from the Midcourse Space Experiment. Processing of the data was funded by the Ballistic Missile Defense Organization with additional support from NASA Office of Space Science. This research has also made use of the NASA/ IPAC Infrared Science Archive, which is operated by the Jet Propulsion Laboratory, California Institute of Technology, under contract with the National Aeronautics and Space Administration.

The present work is based on observations with ISO, an ESA project with instruments funded by ESA Member States (especially the PI countries: France, Germany, the Netherlands and the United Kingdom) and with the participation of ISAS and NASA.

## References

- Allamandola L.J., Hudgins D.M., Sandford S.A., 1999, ApJ, 511, L115
- Allamandola L.J., Tielens A.G.M.M., Barker J.R., 1985, ApJ, 290, L25
- Borghesi A., Bussoletti E., Colangeli L., 1987, ApJ, 314, 422
- Césarsky C.J., Abergel A., Agnese P., et al., 1996, A&A, 315, L32
- Cohen M., 1999, in “New Perspectives on the Interstellar Medium”, ASP Conf. Series, Vol. 168, p97



- Cohen M, Green A.J., 2001, MNRAS, 325, 531
- Cr  t   E., Giard M., Joblin C., Vauglin I., L  ger A., Rouan D., 1999, A&A, 352, 277
- Draine B.T., Lee H.M., 1984, ApJ, 285, 89
- Egan M.P., et al. 1999, *MSX Point Source Catalog Explanatory Guide*, AFRL-VS-TR-1999-1522
- Joblin C., Tielens A.G.G.M., Geballe T.R., Wooden D.H., 1996, ApJ, 460, L119
- Leger A., Puget J.L., 1984, A&A, 137, L5
- Mathis J.S., 1990, ARAA, 28, 37
- Mathis J.S., Rumpl W., Nordsieck K.H., 1977, ApJ, 217, 425
- Mezger P. G., Mathis J.S., Panagia N., 1982, A&A, 105, 327
- Mookerjee B., Ghosh S.K., 1999, JA&A, 20, 1
- Mookerjee B., Ghosh S.K., Karnik A.D., Rengarajan T.N., Tandon S.N., Verma R.P., 1999, ApJ, 522, 285
- Price S.D., Egan M.P., Carey S.J., Mizuno D.R., Kuchar T.A., 2001, AJ, 121, 2819
- Sakata A., Wada S., Tanabe T., Onaka T., 1984, ApJ, 287, L51
- Savage B.D., Mathis J.S., 1979, ARAA, 17, 73
- Scoville N.Z., Kwan J., 1976, ApJ, 206, 718
- Verstraete L., Pech C., Moutou C., Sellgren K., Wright C.M., Giard M., Leger A., Timmermann R., Drapatz, S., 2001, A&A, 372, 981
- Zavagno A., Ducci V., 2001, A&A, 371, 312 (ZD)